Annual Report

A Framework for the Seismic Risk Assessment of Masonry Arch Bridges in the United States

Aditya Kamath[1], Saurabh Prabhu[2] & Sez Atamturktur[3]

July, 2018

[1] Structural Engineer, Enercon Services, akamath@enercon.com
(Previously, Graduate Student in the Glenn Department of Civil Engineering at Clemson University)

[2] Senior Catastrophe Research Analyst, AIG, saurabh.prabhu@aig.com
(Previously, Post-doctoral Fellow in the Glenn Department of Civil Engineering at Clemson University)

[3] Harry and Arlene Schell Professor & Head of the Department of Architectural Engineering, The Pennsylvania State University, sez@psu.edu (Principal investigator)
(Previously, Provost's Distinguished Professor, Department of Mechanical Engineering, Clemson University)

Abstract

Primarily constructed at the turn of the 20th century, over 1600 masonry arch bridges continue to serve as part of the U.S. transportation infrastructure. The preservation of these bridges is important for not only their role in the transportation network but also their cultural and architectural value. For successful preservation, the stewards of these historical bridges must be equipped with tools to evaluate the bridge vulnerability to extreme events and to make risk-aware decisions about their preservation and maintenance. To this end, focusing specifically on earthquakes, the current study presents a framework to calculate *seismic risk indices* for masonry arch bridges in the U.S. The risk indices are estimated first by developing non-linear finite element models and next by using those models to conduct fragility analysis under seismic excitation. The framework presented herein, if implemented for all site-appropriate hazard scenarios, can aid in the development of retrofitting strategies that will minimize risk, reduce financial loss, and ensure the preservation of the historically valuable bridges.

Keywords: finite element analysis, risk assessment, masonry arch bridges, heritage structures, non-linear analysis, fragility curves

1. Introduction

The United States has more than 1600 masonry arch bridges in its transportation network, nearly half of which are over 100 years old (Figure 1) (Citto & Woodham, 2015). Over the course of their lifetime, these bridges have inevitably deteriorated, and their load-carrying capacity has decreased as a result of natural aging, such as weathering, freeze-thaw cycles, and biodegradation (Chajes, 2002). Compounding this situation is the limited state-of-the-art knowledge about engineering design at the time of the bridges' construction. The masonry arch was a widely used construction technique at the turn of the 20th century, a time when bridge design criteria primarily focused on static gravitational loads and neglected dynamic seismic effects (Santis, 2011; Pellegrino et al., 2014; Porto et al., 2016). Additionally, an increase in average traffic loads over the last century has caused masonry arch bridges to sustain gravitational loads far beyond those calculated by their builders (Loo & Yang, 1991; NG, 1999; Wu, 2010; Sarhosis et al., 2016). Despite these issues, many masonry arch bridges remain in service because of their high replacement costs and/or their historic designation (Citto & Woodham, 2015).

Figure 1 : Location of masonry arch bridges in the United States and the corresponding seismic hazard.

Damage compromising the structural integrity of masonry arch bridges can significantly hinder the transportation network, cause traffic disruptions, and impede evacuation and first-response efforts after a disaster (Basoz and Kiremidjian, 1997; Lu et al. 2016). Because masonry arch bridges continue to play an integral role in the U.S. transportation network, it is imperative to consider how they might be affected by extreme events, such as earthquakes. In the aftermath of seismic activity, masonry arch bridges have been observed to develop in-plane four-hinge mechanism or an out-of-plane mechanism involving rotation of a spandrel wall that lead to bridge collapse (Dejong, 2009; Santis, 2011; Scheibmeir, 2012; Prabhu and Atamturktur 2013; Zampieri et al., 2016). In Italy, for instance, the 1997 Umbria and Marche earthquake caused the collapse of the spandrel walls of several masonry arch bridges (Bhatti, 2009), while the 2001 Bhuj earthquake in western India caused rotation of several bridges' spandrel walls, which resulted in the collapse of the bridge backfill material (Ghosh, 2001; Rota, 2004). In addition, the 2008 Wenchuan earthquake in the Sichuan province of China resulted in the failure of the arch support system (and

ultimately the complete collapse) of the Yingchuan Bridge (Kawashima et al., 2008), while a 2016 earthquake in Kumamoto, Japan, led to the collapse of the spandrel walls of several Japanese masonry arch bridges (Iwaki et al., 2016). These recent events highlight the need for and importance of seismic assessment of masonry arch bridges (Zampieri et al., 2015; Tecchio et al., 2016).

In this paper, the authors present a framework to enable risk-based decision-making as it relates to disaster preparedness: the restoration and rehabilitation of U.S. masonry arch bridges. Focusing on *single-span* bridges, which form the largest group (44%) within the U.S. masonry arch bridge inventory, this research develops seismic risk indices that combine the seismic fragility of bridge types and the seismic hazards of geographical areas. Seismic fragility analysis calculates the probability of reaching or exceeding a given level of damage when a structure is subjected to a range of ground motion intensities (King et al., 1997; Calvi et al., 2006; Nielson, 2006). Fragility curves are calculated for 20 bridge archetypes that are representative of the U.S. single-span masonry arch bridge inventory.

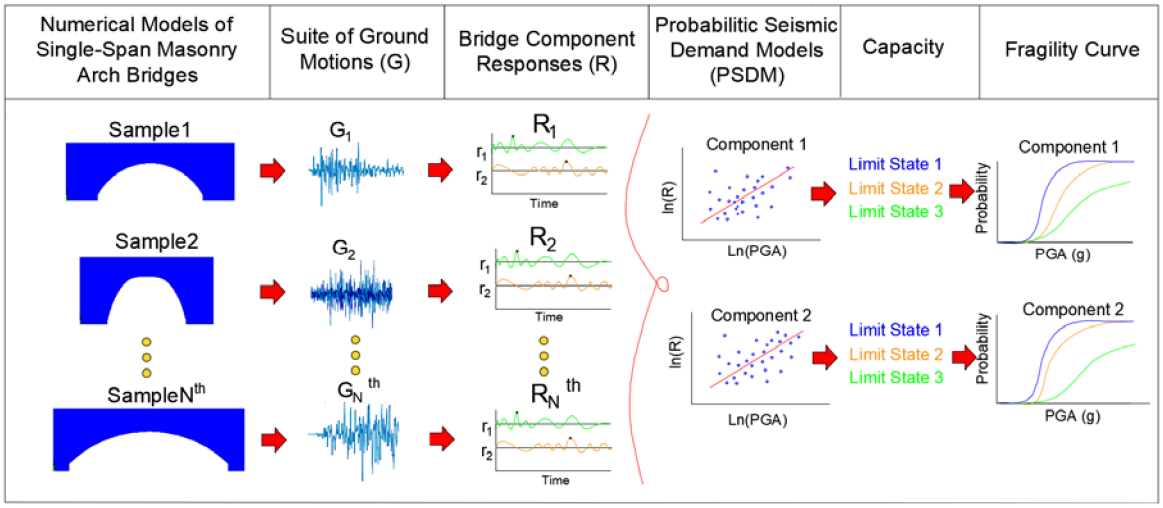

Figure 2 : Methodology for generating fragility curves using non-linear time history analysis

The process utilized in this study to calculate the fragility curves is shown in Figure 2. The process is composed of multiple steps. The authors begin by analyzing the National Bridge Inventory (NBI) database to obtain and categorize geometric data for existing masonry arch bridges. Using this data, we generate *N* distinct masonry arch bridge archetypes by sampling the material property values of bridge components. Next, we obtain a suite of ground motions appropriate to the geographic regions of interest. We randomly pair these ground motion records with bridge archetypes through a Monte Carlo simulation and subsequently perform a non-linear time history analysis. We then generate a probabilistic seismic demand model using the peak response for key components identified through the non-linear time history analysis, and we determine the limit state for each bridge component to generate a capacity model. Finally, we

generate fragility curves based on differences between bridge demand and capacity, and we calculate risk indices by combining the fragility of each bridge archetype with local seismic hazards.

This paper is organized as follows: Section 2 discusses the processes used to obtain geometric properties for existing single-span arch bridges in the U.S.; these properties are then used to generate representative bridge archetypes. Section 3 presents the development of finite element (FE) models for the aforementioned archetypes. Section 4 discusses seismic hazards in different regions of the U.S., the development of synthetic ground motion records for the performance of non-linear time history analysis, and the identification of appropriate collapse mechanisms for generating this study's fragility curves. Section 5 discusses the methodology used to calculate the fragility curves, while Section 6 presents the risk indices estimated for the nation's existing single-span masonry arch bridges. Finally, Section 7 summarizes the study, reviews the findings, and discusses areas for future work.

2. Analysis of the National Bridge Inventory (NBI) and Archetype Development

2.1 Single-Span Masonry Arch Bridge Inventory

As Figure 3 illustrates, a single-span masonry arch bridge consists of four major components (see the emboldened terms in the figure): backfill, an arch vault, abutments, and spandrel walls. The backfill, which typically consists of dry stone, coarse aggregate, sand or ballast (Ural et al. 2008; Bhatti, 2009), acts as a medium for distributing the vertical loads from the road pavement to the arch vault. The backfill itself is constrained by the spandrel walls, which provide structural integrity (Fanning et al., 2001; Rota et al., 2005). Meanwhile, the arch vault distributes the aforementioned vertical loads to the abutments and the ground in the form of horizontal and vertical thrust (Fanning et al. 2001). The rise-to-span ratio of the arch vault influences the ratio between the horizontal and vertical thrusts (Bhatti, 2009; Atamturktur et al. 2013; Zampieri et al., 2014). Finally, the abutments, which typically consist of massive stone blocks, transfer the vertical loads to the surrounding ground.

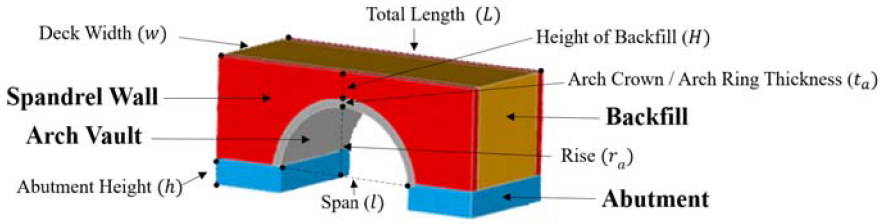

Figure 3 : Components of a single-span masonry arch bridge.

Each of the four main components of a single-span masonry arch bridge directly contributes to the stiffness and strength of the bridge system and must therefore be included in any numerical model developed for seismic analysis. Geometric parameters associated with these components include the rise of the arch (r_a), the span length (Z), the deck width (w), the abutment height (h), the thickness of the arch ring (t_a), the total length of the bridge (L), and the height of the backfill above the arch (H) (Figure 3).

To obtain the geometric properties for existing U.S. masonry arch bridges, the authors consulted the National Bridge Inventory (NBI), a database maintained by the Federal Highway Administration, which features data related to over 600,000 highway bridges in the U.S. (FHWA, 2012). The NBI was used to obtain information about 744 single-span masonry arch bridges. In particular, the database provided information about the bridges' number of spans, span length, width, construction year, and geographic location. For the purpose of developing numerical models of masonry arch bridges, the authors derived other pertinent information (e.g., arch rise, abutment height, thickness of the arch, and total length and height of the backfill above the arch) using photographic evidence. Such evidence was available for 326 of the 744 bridges. However, only 150 of the 326 photographs enabled observation of the thickness of the bridges' arch rings. Based on the available geometric data from these 150 bridges, a regression model was constructed to predict arch thickness for a given arch span ($t_a = 0.0405 * I + 0.296$, $R^2 = 0.37$). This model was then used to assign the values of t_a to the remaining 176 bridges.

2.2 Clustering of Representative Bridge Archetypes

Figure 4 illustrates the distribution of the geometric properties obtained for the 326 single-span masonry arch bridges, as well as the number of bridges constructed during any given year. In this study, the authors used a *k-means* clustering technique to cluster the existing bridges into 20 representative bridge archetypes based on their geometric parameters (Hartigan and Wong, 1979). The purpose of this clustering was to reduce the number of bridge models needed for evaluation and thus to reduce the number of simulation runs and the corresponding computational effort.

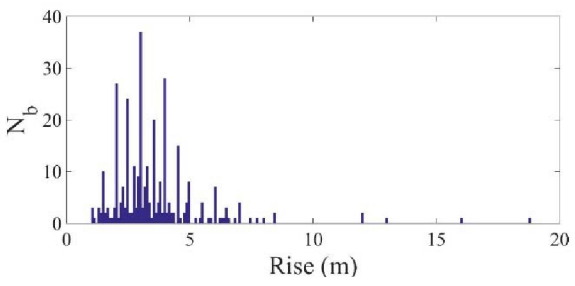

a)

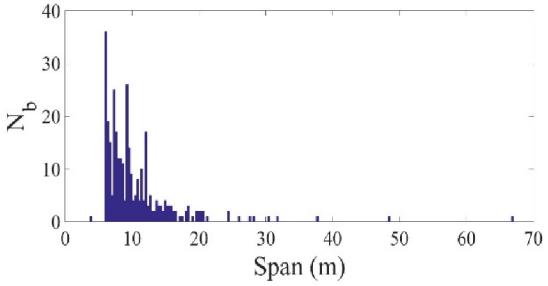

b)

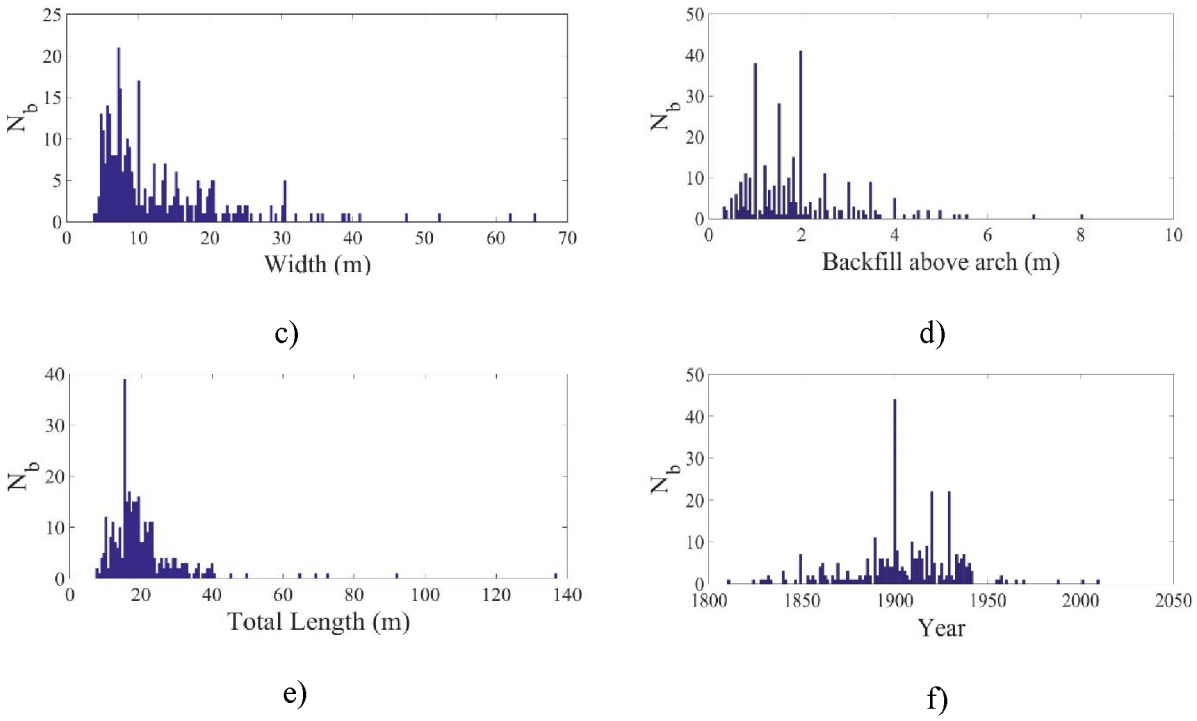

Figure 4 : Distribution of characteristics of single-span masonry arch bridges in the U.S. a) rise b) span, c) width, d) height of backfill above arch, e) total length, f) construction year. N_b is the number of bridges.

k-means clustering involves an iterative process of placing a user-defined number of clusters in a parameter space and calculating the distance between each cluster's centroid and each data point within the relevant cluster (Hartigan and Wong, 1979). These two steps are repeated in an iterative manner to adjust the positions of clusters in such a way that the summation of squared error (see Eq. 1) is kept at a minimum.

$$\sum_{i=1}^{K} \sum_{x_i \in c_i}^{n_i} \|x_i - \mu_i\|^2 \tag{1}$$

In Eq. 1, x_t represents the location of the data points corresponding to centroid q, μ_i is the mean of all data points belonging to the cluster with centroid c_t; Hj represents the total number of data points corresponding to q; and K represents the total number of clusters.

To select the optimal number of clusters, the authors adapted the widely used approach known as the elbow method (Kodinariya and Makwana, 2013). In this method, variance is defined as the ratio of the variance between the clusters (see Eq. 2) and the total variance of the geometric dataset (see Eq. 3).

$$\sum_{i=1}^{K} K * (c_i - x_M)^2 \quad (2)$$

$$\sum (x - x_M)^2 \quad (3)$$

In Equations 2 and 3, c_t represents the centroid of a cluster; x_M represents the mean of the geometric dataset (i.e., $\frac{\sum x}{N}$); x represents the geometric data points; and N is the total number of data points. In the elbow method, the number of clusters, K is gradually increased, and the variance is repeatedly calculated until the graph of the clusters converges to a plateau. Figure 5 shows the change in variance increasing numbers of clusters related to the geometric dataset compiled in the previous section. When 20 clusters were used (i.e., when the variance reached 90 %), the graph of the clusters started to plateau, which suggested that additional clusters would make an insignificant difference in the variance. For this reason, the author's selected 20 representative single-span masonry arch bridges as archetypes for fragility analysis (see Table 1).

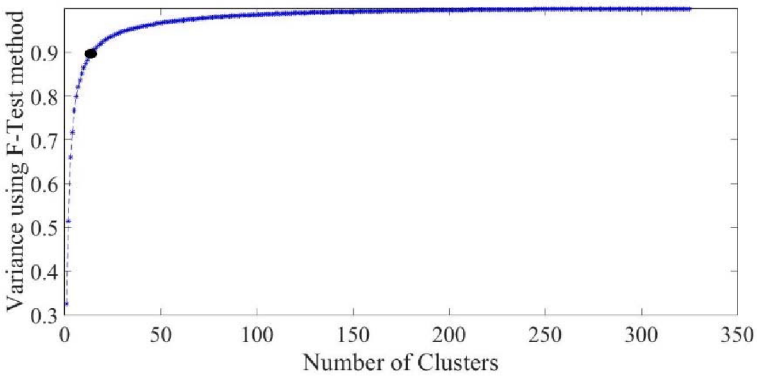

Figure 5 : The elbow approach to determine the optimal number of clusters for 326 existing single-span masonry arch bridges.

3. Numerical Model Development

This section discusses the development of FE models for the 20 bridge archetypes. In what follows, we review the geometric representation and solid modeling of the archetypal bridges, the selection of element types, the idealization of support conditions, and the definition of material properties. In addition, we discuss the mesh refinement study used to determine a suitable trade-off between numerical accuracy and computational demand.

3.1 Geometric Representation of Archetypes

For the 20 representative bridge archetypes considered in this study, each of the geometric property values was set at the mean value of the corresponding parameter in a cluster (i.e., the centroid of each cluster) (see Table 1 for the parameters). Using these geometric property values,

finite elements models for the 20 bridge archetypes were then developed in ANSYS v.17. A macro-modeling approach was adopted, which involved modeling the masonry as a single continuum without any mortar joints (Lourenco et al., 2002; Atamturktur et al. 2012; Li et al. 2014).

Table 1: Geometric properties of 20 representative bridge archetypes obtained using the *k-means* clustering technique.

Archetype	Span (m)	Total Length (m)	Rise (m)	Width (m)	Backfill (m)	Arch Thickness (m)	Abutment Height (m)
1	11.41	19.45	4.19	5.93	1.66	0.72	0.82
2	15.86	30.92	4.40	13.93	1.65	0.85	1.03
3	8.70	17.04	3.27	59.87	1.63	0.63	1.23
4	17.97	24.97	4.03	30.00	1.93	0.97	0.77
5	13.40	34.74	5.81	24.37	4.01	0.70	3.33
6	7.48	15.30	2.66	18.82	1.57	0.61	0.34
7	9.39	36.27	4.10	10.43	2.46	0.67	2.66
8	67.00	137.10	18.83	5.30	8.05	2.50	1.20
9	12.49	19.09	3.00	38.78	1.59	0.75	2.32
10	8.51	16.07	2.96	13.06	1.88	0.63	0.68
11	9.44	17.36	3.48	27.25	1.64	0.68	1.27
12	8.36	23.78	3.21	7.97	1.49	0.58	0.65
13	12.20	92.20	5.80	9.40	4.50	1.50	1.00
14	8.10	14.10	3.56	21.06	3.02	0.61	3.06
15	13.37	20.23	3.97	18.38	2.19	0.67	1.49
16	19.92	46.08	7.52	7.70	2.38	0.95	0.42
17	7.10	14.62	2.69	7.29	1.52	0.60	0.70
18	21.95	31.61	5.42	8.91	2.65	1.10	1.15
19	43.15	66.75	10.75	13.85	2.50	2.04	3.00
20	7.00	15.06	2.98	9.65	1.64	0.65	1.02

3.2 Material Models

The masonry assembly of the arch, the abutments, and the spandrel walls were modeled as a homogenous solid, and a smeared cracking analogy was used to approximate the cracking and crushing behavior of the material in the presence of seismic activity (ANSYS, 2010; Prabhu et al. 2014). These approximations were achieved by implementing the SOLID65 element to represent the soil backfill and the masonry assembly of the bridge archetypes (Figure 8). SOLID65, an 8-noded isoparametric hexahedron element with three translational degrees of freedom at each node, has been widely used for both dynamic and non-linear static analysis of masonry assemblies in ANSYS v.17 (Fanning & Boothby, 2001; Andreas et al., 2002; Taghikhany et al., 2008; Sevim et al., 2011; Li, 2012; Musmar et al., 2013; Zhang, 2015; Betti et al., 2015; Prabhu et al. 2015). SOLID65 is capable both of cracking in tension using a smeared crack analogy and of crushing in

compression through a plasticity algorithm based on the Willam-Warnke yield criteria (William and Warnke, 1975). The element cracks or crushes at its integration points as soon as the principal stresses lie outside the failure surface. Cracked or crushed regions are formed perpendicularly to the relevant principal stress direction, and the stresses are redistributed locally. By assigning a shear transfer coefficient for open and closed cracks, SOLID65 can also account for the transfer of shear loads across a crack. The said transfer results from interlocking effects. The plasticity of the masonry assembly prior to cracking/crushing can be accounted for by adopting the Drucker-Prager material model (Drucker & Prager, 1952; Fanning and Boothby, 2001; Li and Atamturktur, 2013). The Drucker-Prager model, widely used in studies of the plasticity of masonry (Wang and Melbourne, 2007; Sevim et al., 2011; Betti and Galano, 2012), is a pressure-dependent model, which means that the elastic, perfectly plastic behavior of the masonry is introduced as soon as the stresses reach the elastic limit state.

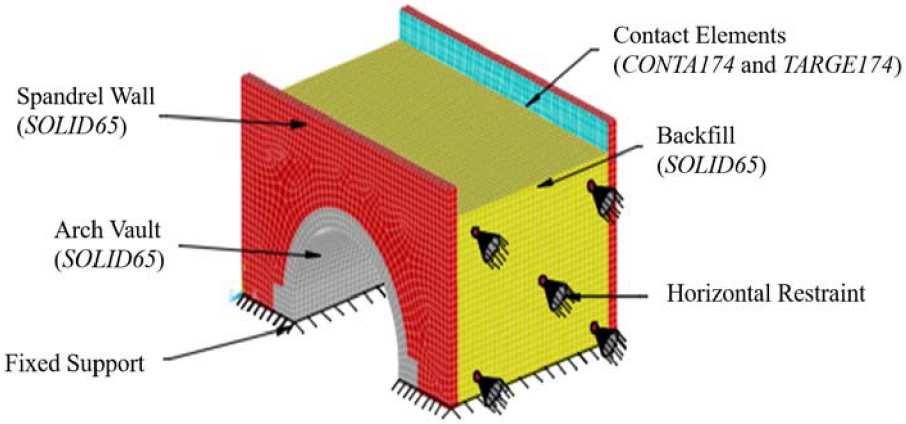

Figure 6 : Element types and support conditions of the FE models of single-span masonry arch bridges.

3.3 Support Conditions

As the arch abutments and the spandrel walls of a masonry arch bridge are usually embedded in the ground, they are idealized to be fixed (NG, 1999; Fanning & Boothby, 2001; Wang & Melbourne, 2007; Sevim et al. 2011; Prabhu et al. 2014). In this study, the backfill at the two ends along the bridge span was assumed to be horizontally restrained by the wing-walls (i.e., retaining walls that are built next to the abutments). The surface interactions at the interface between the backfill soil and the masonry assembly (i.e., the spandrel walls, arch vault, and abutments) were captured using 8-noded CONTAC175 and TARGE170 elements. These elements have three translational degrees of freedom at each node and were located over the surface of SOLID65 elements. The contact and target element pair prevented penetration at the interface while allowing sliding; in this fashion, the relative movement between masonry and soil was taken into account. This sliding behavior was governed by a combination of several factors, including friction and cohesion, both of which were idealized with coefficients specified in the next subsection.

3.4 Material Properties of the Masonry Assembly

The probability distributions for the material property values of the masonry assembly and the soil backfill were defined based on the pertinent literature. For the masonry assembly, the modulus of elasticity was represented with a uniform distribution, with values ranging from 1 – 15 Gpa. Per the recommendation of the American Society for Testing and Materials (ASTM), the density of stone masonry is normally distributed with a mean of 2360 *kg*/m^3 and a standard deviation of 139 *kg/m*^{3}. The compressive strength of stone masonry is assumed to be uniformly distributed in the range of 5 Mpa to 10 Mpa (Fanning & Boothby, 2001).

In this study, the plasticity of stone masonry was defined using the two parameters of the Drucker-Prager model: cohesion (*c*) and internal friction angle (0). The values for these coefficients were determined according to Sarhosis et al. (2016) as $c = 0.1065 * /_c' + 0.531$ and $0 = 0.145* /_c' +49.71$, where $/_c'$ represents the compressive strength of the masonry in Mpa. Meanwhile, the shear transfer coefficient for an open crack in the masonry was assigned a mean value of 0.4 and a standard deviation of 0.05, and the shear transfer coefficient for a closed crack was assigned a mean value of 0.95 and a standard deviation of 0.025 (Wang, 2004).

The modulus of elasticity of the backfill soil was assumed to have a uniform distribution, with values ranging from 2 MPA to 200 MPa. In addition, the density of the soil was normally distributed with a mean value of 1800 /qy/m^3 and a standard deviation of 50 /fcg/m^3 (Oliveira et al., 2010; Pela et al., 2009). Finally, the cohesion coefficient, *c*, was accepted to have uniform distribution with values ranging from 10^{-3}MPa to 0.1 MPa.

As regards friction, the internal friction angle (0) was assigned a mean value of 35.2 degrees and a standard deviation of 0.5 degrees (FHWA, 2002). Moreover, the friction coefficient of the contact surface between the soil backfill and the masonry assembly was defined as a uniform distribution with values ranging from 0.3 to 0.9 (Wang & Melbourne, 2007; Prabhu et al. 2014) and a contact stiffness factor of 0.1 (Fanning & Boothby, 2001; Wang & Melbourne, 2007).

3.5 Mesh Refinement Investigation

To determine an appropriate mesh discretization, one that offered an acceptable trade-off between solution accuracy and computational time, a mesh refinement investigation was conducted. In this investigation, the level of discretization was varied from coarse to fine as the solution accuracy was monitored for response quantities of interest (Hughes et al., 2005). Deflection of the arch vault of the bridge at the mid-span under gravity loads was chosen as the response quantity of interest for the mesh refinement investigation. A linear analysis was conducted, and the deflection of the center node of the arch vault was monitored as the average element size was repeatedly decreased. When the average element *size* was decreased, the *number*

of elements correspondingly increased. For example, for bridge archetype 20 (shown in Fig. 7), the authors observed that lowering the element size from 0.25 m to 0.15 m yielded only a 5% change between the number of finite elements in the solutions. Because this percentage difference was assumed appropriate in this study, an element size of 0.25 m was implemented in the numerical analysis in the rest of the study.

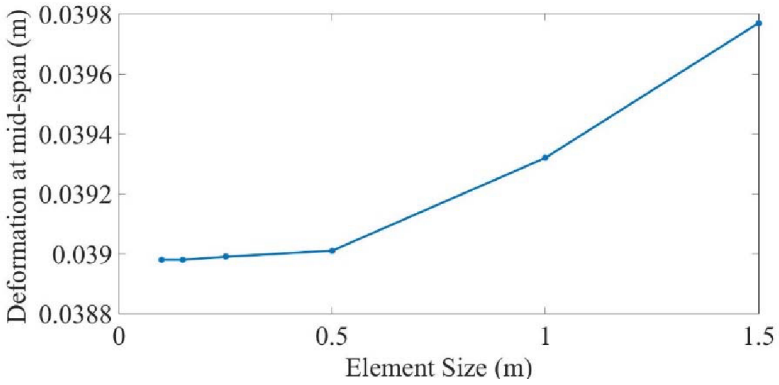

Figure 7 : Mesh refinement study to select the optimal number of finite elements for bridge archetype 20

4. Obtaining Ground Motion Records and Determining Damage Limit States

4.1 Ground Motion Records

The seismic hazards for different regions of the U.S. are characterized in the National Seismic Hazard Models developed by the United States Geological Survey (USGS). These models are widely used for the seismic risk assessment of bridges, highways, buildings, and other structures. Among the products created by the USGS are maps that indicate the *probability* of seismic hazard (USGS, 2016). Figure 10 provides two seismic hazard maps, both of which focus on the central and eastern regions of the U.S. (i.e., the regions where the majority of masonry arch bridges are located). The first map in the figure illustrates peak ground acceleration (PGA) with a 2% probability of exceedance in 50 years, and the second illustrates PGA with a 10% probability of exceedance during that same time period.

Fragility analysis, discussed in detail in Section 5, requires selecting an intensity measure (IM), such as PGA or Spectral Acceleration, S_a. The selected IM should have a strong correlation with the response of the structure to seismic activity and should be applicable to bridge archetypes. In this study, PGA was selected as the IM. It has been widely used for vulnerability assessment of structures in past studies (Kim & Shinozuka, 2004; Field, 2005). Padgett et al. (2008) have suggested that PGA is an optimal IM for probabilistic seismic demand models because of its efficiency, practicality, sufficiency, and hazard computability.

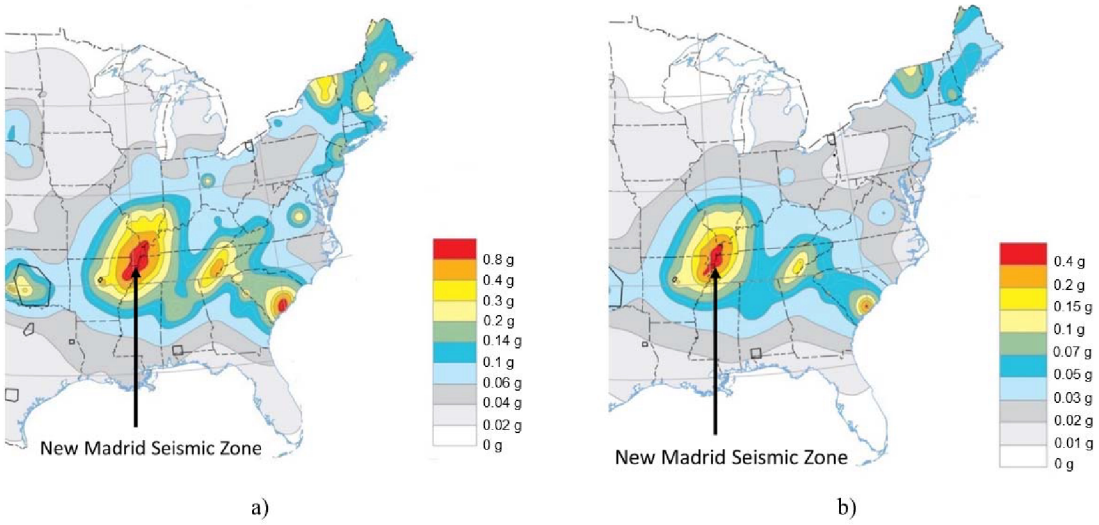

Figure 8 : Peak ground acceleration in the central and eastern U.S with, a) 2% probability of exceedance in 50 years and b) 10% probability of exceedance in 50 years (USGS, 2016).

As shown earlier in Figure 1, the majority of masonry arch bridges are located in the central and northeastern U.S. To assess seismic vulnerability of these bridges, it is important to use ground motion records that are representative of these regions. In addition, we also need to have a large enough number of records to provide an accurate characterization of the potential responses (e.g., stress, strain, deformation) of bridge components to a given earthquake (Santis, 2011). Although there are several databases of past earthquake ground motion records and their corresponding time-acceleration records maintained by the Pacific Earthquake Engineering Research Center (PEER) and the Federal Emergency Management Agency (FEMA) for fragility analyses, these ground motion records are derived using earthquake records from the western regions of the U.S, and are primarily intended towards buildings with natural periods less than 4 sec. In the case of the central and northeastern U.S., ground motion records are limited. The option of using scale factors to the actual ground motion records to obtain the desired earthquake scenario is not applicable as demonstrated by Luco and Bazzurro (2007), since scaled ground motions may fail to represent the true characteristics of an earthquake scenario in the central and northeastern U.S.

Accordingly, for our study, we deemed appropriate to employ synthetic ground motions, which reproduce characteristics of earthquakes in the central and northeastern U.S. The use of similar synthetic ground motions as an alternative to measured ground motion records is commonplace in seismic assessment of civil infrastructure (Boore, 2003; Mavroeidis and Papageorgiou, 2004; Sanaz and Kiureghian, 2010; Rezaeian and Kiureghian, 2010). In particular, we employ the synthetic ground motions generated by Wen & Wu (2001) for Memphis, Tennessee, St. Louis, Missouri, and Carbondale, Illinois, using stochastic ground motion simulation methods and the latest seismicity information from the New Madrid Seismic Zone (NMSZ), a highly active region in the central U.S. (see Fig. 8). In their study, Wen & Wu (2001) developed a suite of 60 total synthetic ground motion records for the three cities within the NMSZ, and the synthetic

records reflected 2% and 10% probability of exceedance in 50 years. As given in Table 2, in developing synthetic ground records, Wen & Wu (2001) considered time-acceleration records, as well as those records' corresponding PGA values and predominant periods of seismic activity. Figure 11 provides the distribution of the PGA values (0.06g to 0.66g) for Wen & Wu's 60 synthetic ground motion records. Although these synthetic ground motions were developed for the NMSZ, it is worth noting that they have been previously adopted for vulnerability assessment of bridges located in the northeastern region of U.S. (Seo, 2009), as it is intended in this study.

Table 2 : Sample time-acceleration records and their corresponding PGAs and predominant periods for Wen & Wu ground motions.

Sample	PGA (g)	Predominant Period (sec)	Time-Acceleration (a) Record
1	0.013	0.22	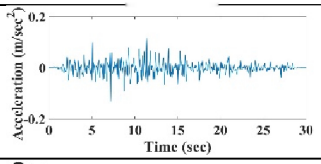
2	0.083	0.18	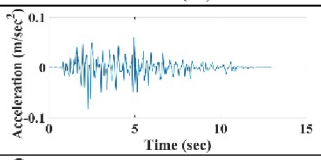
3	0.322	0.26	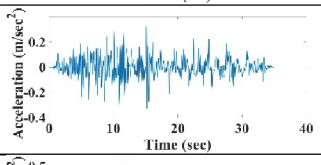
4	0.485	0.8	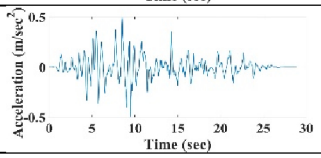

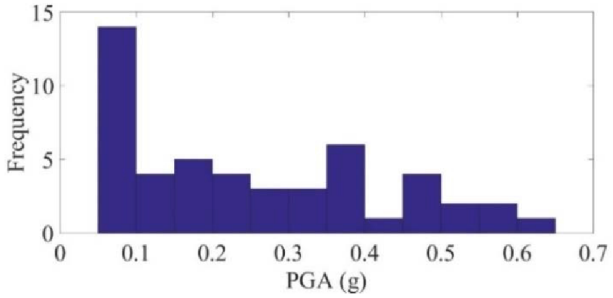

Figure 9 : The distribution of PGA values for the Wen & Wu (2001) ground motions.

4.2 Limit States

According to Santis (2011), seismic damage to the components of single-span masonry arch bridges can be classified according to the type of collapse mechanism or the severity of the damage. In this study, two collapse mechanisms were selected based on observed damage under seismic loads and the loads' influence on the structural functionality of the bridge after damage (Zampieri et al., 2016; Tecchio et al., 2016; Sarhosis, et al., 2016). The selected mechanisms were i) the relative displacement of the arch crown (i.e., the top of the arch vaults) and the abutment and ii) the rotation of the spandrel walls.

The first collapse mechanism is formed when the arch vault, subjected to longitudinal seismic loads, fails as a result of the formation of a four-hinge mechanism (see Fig. 12). The second collapse mechanism is formed when the spandrel walls rotate as a result of transverse seismic loads (see Fig. 13) (Tecchio et al., 2012; Zampieri et al., 2014). In this study, demand measures fragility analysis were thus selected for longitudinal and transverse loads. In the case of the former, the selected demand measure was the relative displacement of the abutment and the arch crown, and in the case of the latter, the selected demand measure was the relative movement of the peak of the spandrel walls with respect to its base.

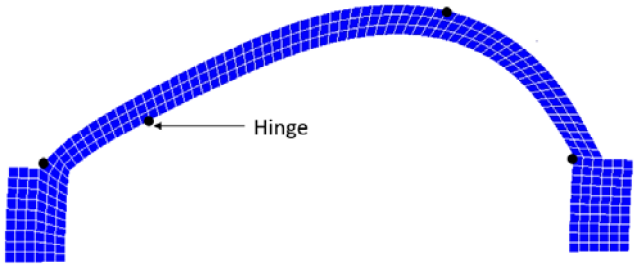

Figure 10 : Formation of a four-hinge mechanism at the arch vault when subjected to longitudinal seismic loads.

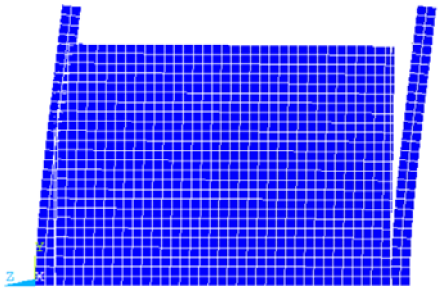

Figure 11 : Rotation of a spandrel wall when subjected to transverse seismic loads

In previous research, significant attention has been paid to damage limit states for concrete buildings and bridges. HAZUS categorizes the damage limit states for concrete bridges in four levels: slight, moderate, extensive, and complete. Each damage state corresponds to particular problems of functionality in a structure or its components (Nielson, 2006; Lagomarsino & Cattari, 2015). No similar categorization of damage states exists for masonry arch bridges, however (Santis, 2011; Zampieri et al., 2016). One major challenge of the current study was thus defining quantitative values for the limit states for historic masonry arch bridges. Previous research has indirectly underscored the difficulty of this challenge as it relates to the current study's two selected collapse mechanisms.

For instance, Theodossopoulous et al. (2003) studied the behavior of masonry bridges' arch vaults by inducing displacement in the bridges' abutments. When an abutment was displaced by 0.3% of the arch span, crack formations were observed; when the displacement was increased to 0.5%, fractures were formed along the arch vault; and when the displacement was additionally increased to 0.8%, plastic deformation and the collapse of the arch occurred. In a related vein, Holzer (2013) found that progressive cracks appeared when an abutment moved by 0.01% of an arch span and that any further abutment movement led to the formation of plastic hinge mechanisms. Meanwhile, Zhang (2015), in conducting a study on a series of masonry arches, found that plastic hinge mechanisms generally started to form at an arch displacement of 0.1% to 0.3% of the arch span. Finally, in their tests on the out-of-plane loading behavior of masonry walls, Bui et al. (2010) found that spandrel walls cracked at a deflection (i.e., rotation) of 0.25% of wall height and then underwent a plastic deformation at about 1% of total height. As these studies indicate when taken together, the two collapse mechanisms selected for the current study are highly dependent on the material, boundary condition and geometric characteristics of the components of a masonry arch. Based on this meta-analysis, the authors thus chose three limit states (i.e., slight, moderate, and extensive), as defined in Table 3.

Table 3: Damage limit states for selected collapse mechanisms: i) relative displacement between arch crown and abutment and ii) rotation of spandrel wall.

Damage Type	**Damage Limit State – 1 (Slight)**	**Damage Limit State – 2 (Moderate)**	**Damage Limit State – 3 (Extensive)**
Relative displacement between arch crown and abutment	0.1% of span	0.2 % of span	0.3% of span
Rotation of spandrel wall	0.25 % of height of wall	0.5 % of height of wall	1.0 % of height of wall

5. Fragility Analysis

Fragility curves give the cumulative probability of exceeding a damage state for a range of hazard intensity measures (Mander & Basoz, 1999; Nielson & DesRoches, 2003; Porter, 2015; Nilsson, 2008; Padgett & DeRoches, 2008; Ramanathan et al., 2010; Lallemant et al., 2015; Tecchio et al., 2016). The conditional probability of exceeding a damage state for a particular intensity measure is given by

$$Fragility = P[D \geq d|IM = y] \tag{4}$$

where D and d represent the seismic demand and damage limit state, respectively, for a given system; where IM is the ground motion intensity measure or peak ground acceleration; and where y is a specific ground motion intensity measure. When no earthquake damage data are available to generate fragility curves for bridges, analytical methods are used (Lang, 2002; Nielson, 2006). Analytical fragility functions are generated using two parameters: structural capacity (C) and structural demand (D). The probability of failure *Pj* is determined using Equation 5:

$$P_f = P[\frac{D}{C} \geq 1] \tag{5}$$

When both seismic demand and structural capacity follow a lognormal distribution, Equation 5 can be reformulated as Equation 6 using the central limit theorem (Melchers, 2001):

$$P[C - D \leq 0.0|IM] = \emptyset[\frac{\ln(S_d/S_c)}{\sqrt{{\beta_c}^2 + {\beta_d}^2}}] \tag{6}$$

where S_d and S_c represent the structural demand and structural capacity of the bridges, respectively; where β_c and fi_d represent the logarithmic standard deviation for structural capacity and structural demand, respectively; and where 0[ ] represents the normal distribution function. The probability function is a lognormal distributed function and has been found to represent structural/non-structural damage data accurately (Porter et al., 2006).

As in many other studies of bridges (Hwang et al., 2000; Mackie and Stojadinovic, 2001; Bignell et al., 2004; Choi et al., 2004; Nielson, 2005), this study's methodology quantifies seismic demand by using regression analysis in combination with the probabilistic seismic demand model (PSDM) developed by Cornell et al. (2002). For this methodology, the estimate of median demand (EDP) is represented by the power model shown in Equation 7 and illustrated in Figure 6.

$$E\widehat{D}P = aIM^b \tag{7}$$

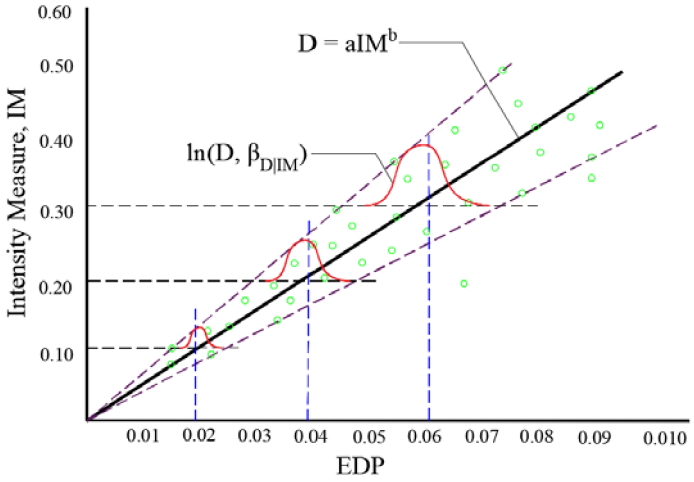

Figure 12 : Probabilistic Seismic Demand Model (PSDM) developed by Cornell et al. (2002)

In Equation 7, IM is the intensity measure, a and b are the regression coefficients, and d represents the limit state. Using the dispersion $Bedpiim$, which is conditional on the IM measure, the PSDM model can be formulated as shown in Equation 8:

$$P[EDP \geq d|IM] = 1 - \phi\left[\frac{\ln(d) - \ln(aIM^b)}{\beta_{EDP|IM}}\right] \quad (8)$$

For mathematical simplicity, the regression coefficients can be derived in a transformed space by taking the natural logarithm of both sides of the equation, which converts Equation 7 into a linear form, as shown in Equation 9:

$$\ln(EDP) = \ln(a) + b \cdot ln(IM) \quad (9)$$

Figure 7 provides an example of natural regression in a transformed space. As the figure illustrates, the variation about the median *Vn(EDP)*, which is given by standard deviation *a*, is the estimate of lognormal standard deviation (dispersion) ,$P_{E}dpiim$ •

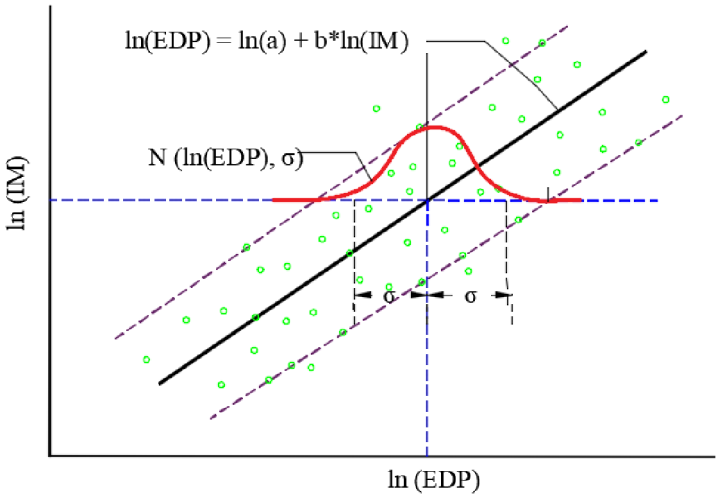

Figure 13 : Illustration of probabilistic seismic demand model in transformed space (Cornell et al., 2002).

Using the PSDM approach, probability of failure *Pj* (Eq. 5) can be rewritten as the probability of reaching or exceeding a limit state for a specific level of demand (EDP), i.e. *P[LSIEDP = y]*. The probability of reaching or exceeding the structural capacity (C) is represented by Equation 10.

$$P_f = 1 - \phi\left[\frac{\ln(d) - \ln(aIM^b)}{\sigma}\right] \tag{10}$$

Equation 10 can be further written, as shown in Equations 11, 12, and 13:

$$= \phi\left[\frac{-\ln(d) + \ln(aIM^b)}{\sigma}\right] \tag{11}$$

$$= \phi\left[\frac{\mathrm{b} * \ln(IM) - (\ln(d) - \ln(a))}{\sigma}\right] \tag{12}$$

$$= \phi\left[\frac{\ln(IM) - \frac{\ln(d) - \ln(a)}{b}}{\frac{\sigma}{b}}\right] \tag{13}$$

Equation 13 can further be further manipulated in the form of Equation 14 as shown below:

$$= \phi\left[\frac{\ln(IM) - \ln(\theta)}{\beta}\right] \tag{14}$$

$$P_f = \emptyset\left[\frac{\ln(IM/\theta)}{\beta}\right] \quad (15)$$

where $\theta = \exp\left(\frac{ln(d)-ln(a)}{b}\right)$, represents the median value of the intensity measure for a given limit state; $\beta = \frac{\sqrt{\sigma^2+\beta_c{}^2}}{b}$ represents the dispersion component for the given limit state; *a* and *b* represent the regression coefficients for the PSDM; *d* represents the value of the given limit state; and ft_c represents the uncertainty (i.e., the dispersion for the capacity limit state). The dispersion is assumed constant at 0.25 based on the recommendation of Nielson (2006).

6. Fragility Analysis of Bridge Archetypes

The response of any structure to seismic loading also depends on the angle of incidence of an earthquake (Nielson, 2006). To account for this uncertainty, the synthetic seismic ground motions developed in this study were applied at random angle *6* ranging from 0 - $\frac{\pi}{2}$ radians, as shown in Figure 14. This range of the angle of incidence was appropriate because of the longitudinal and transverse symmetries of masonry arch bridges.

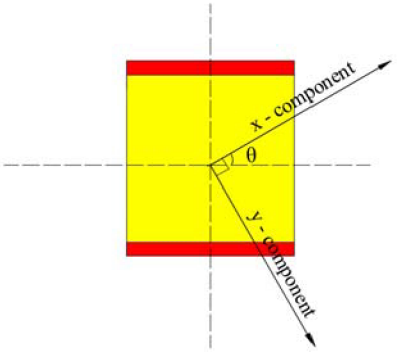

Figure 14 : Seismic ground motion at angle of incidence

Next, a Monte Carlo simulation was conducted with N=2000 combinations of bridge archetypes, each of which was assigned random material properties from its respective distribution. These archetypes were further assigned random ground motions for non-linear dynamic analysis. Next, the PSDM equation (Eq. 7) was calculated for each bridge archetype in connection with the two collapse (i.e., response) mechanisms previously mentioned. Table 4 presents the PSDM equation for each archetype as it relates to the relative movement between

abutment and arch crown, and Table 5 presents the PSDM equation for each archetype as it relates to the rotation of spandrel walls.

Table 4: Probability Seismic Demand Model (PSDM) equations for the 20 bridge archetypes in connection with the relative displacement of abutment and arch crown.

Bridge Archetype	**Relative Displacement of Abutment and Arch Crown (mm)**		
	PSDM		
Type 1	ln(EDP) = 1.0999*ln(PGA) + 3.28	0.4427	1.093
Type 2	ln(EDP) = 1.0392*ln(PGA) + 3.345	0.4449	0.2881
Type 3	ln(EDP) = 1.26*ln(PGA) + 3.5814	0.39	0.5298
Type 4	ln(EDP) = 1.5193*ln(PGA) + 3.3935	0.4713	0.7707
Type 5	ln(EDP) = 1.195*ln(PGA) + 3.8848	0.5028	0.702
Type 6	ln(EDP) = 1.703*ln(PGA) + 3.6509	0.4793	1.162
Type 7	ln(EDP) = 0.885*ln(PGA) + 3.2045	0.4282	0.805
Type 8	ln(EDP) = 0.7473*ln(PGA) + 4.1997	0.3135	0.1475
Type 9	ln(EDP) = 2.1496*ln(PGA) + 4.6035	0.7508	1.314
Type 10	ln(EDP) = 1.027*ln(PGA) + 2.8807	0.2251	0.3642
Type 11	ln(EDP) = 1.4521*ln(PGA) + 3.2802	0.5665	0.3268
Type 12	ln(EDP) = 1.3209*ln(PGA) + 3.1612	0.4695	1.1314
Type 13	ln(EDP) = 0.8657*ln(PGA) + 3.7595	0.4862	0.4279
Type 14	ln(EDP) = 2.224*ln(PGA) + 4.1027	0.5517	0.875
Type 15	ln(EDP) = 1.5034*ln(PGA) + 3.7916	0.546	1.111
Type 16	ln(EDP) = 0.7753*ln(PGA) + 3.3086	0.3665	0.5163
Type 17	ln(EDP) = 0.962*ln(PGA) + 3.806	0.406	0.5497
Type 18	ln(EDP) = 1.0827*ln(PGA) + 4.1009	0.7863	0.1972
Type 19	ln(EDP) = 1.0514*ln(PGA) + 4.1089	0.8617	0.3193
Type 20	ln(EDP) = 1.326*ln(PGA) + 4.0943	0.4751	0.7707

Table 5: Probability Seismic Demand Model (PSDM) equations for the 20 bridge archetypes in connection with spandrel-wall rotation.

Bridge Archetype	**Rotation of Spandrel Wall (mm)**		
	PSDM		
Type 1	ln(EDP) = 1.6807*ln(PGA) + 6.075	0.5974	0.56518
Type 2	ln(EDP) = 1.1962*ln(PGA) + 6.3212	0.3349	0.2881
Type 3	ln(EDP) = 1.4083*ln(PGA) + 4.1396	0.4234	1.2848
Type 4	ln(EDP) = 1.6477*ln(PGA) + 5.5862	0.6082	0.7707

Type 5	ln(EDP) = 1.1181*ln(PGA) + 5.1849	0.573	0.2811
Type 6	ln(EDP) = 1.5031*ln(PGA) + 5.4136	0.5367	0.4897
Type 7	ln(EDP) = 0.9241*ln(PGA) + 6.639	0.4482	0.1834
Type 8	ln(EDP) = 1.1104*ln(PGA) + 8.1203	0.6253	0.1475
Type 9	ln(EDP) = 2.1961*ln(PGA) + 7.1978	0.6275	0.4563
Type 10	ln(EDP) = 1.1931*ln(PGA) + 5.1648	0.3786	0.3642
Type 11	ln(EDP) = 1.2367*ln(PGA) + 5.4592	0.5665	0.3268
Type 12	ln(EDP) = 1.537*ln(PGA) + 6.3619	0.6215	0.3256
Type 13	ln(EDP) = 1.0676*ln(PGA) + 7.7896	0.5005	0.1632
Type 14	ln(EDP) = 1.4862*ln(PGA) + 5.6127	0.5192	0.3746
Type 15	ln(EDP) = 1.4252*ln(PGA) + 6.1333	0.5049	0.3031
Type 16	ln(EDP) = 0.8075*ln(PGA) + 6.8491	0.3947	0.1666
Type 17	ln(EDP) = 1.3679*ln(PGA) + 5.3029	0.5937	0.3902
Type 18	ln(EDP) = 1.3439*ln(PGA) + 6.4131	0.4423	0.355
Type 19	ln(EDP) = 0.7381*ln(PGA) + 7.2703	0.4638	0.1286
Type 20	ln(EDP) = 1.1033*ln(PGA) + 4.4087	0.3168	0.4498

The PSDM equations for each bridge archetype were combined with the given limit state (*d*) to generate fragility curves for slight, moderate, and extensive damage states. Figure 15 shows the fragility curves for bridge archetype 4 as the archetype relates to the collapse mechanisms of i) the displacement between the arch crown and the abutment and ii) the rotation of the spandrel wall.

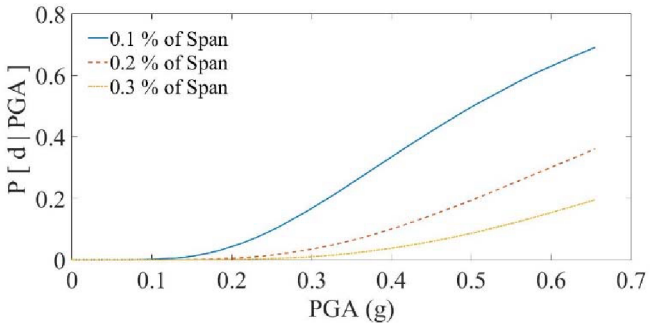

a)

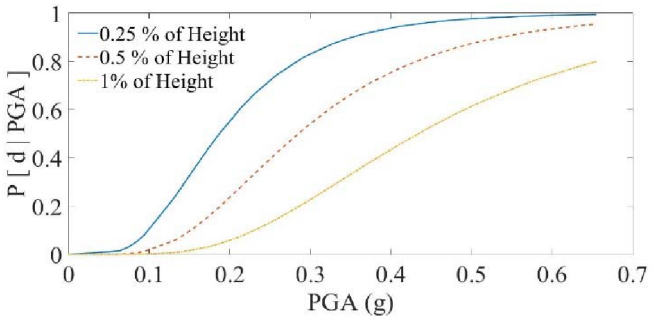

b)

Figure 15 : Example of fragility curves for bridge archetype 4, featuring the three damage states for a) relative displacement between arch crown and abutment and b) rotation of spandrel wall.

The fragility curves generated using the PSDM approach are verified using the Maximum Likelihood Estimation (MLE) approach. The MLE method is based on finding parameter values for 0 and B that maximize the likelihood of predicting the characteristics of the statistical model (Fisher, 1997). Figure 16 provides a comparison of the two fragility curves (i.e., PSDM-generated and MLE-generated) for bridge archetype 1 as it relates to the collapse mechanism of rotating spandrel walls. A comparison of the curves generated by the two approaches shows a maximum discrepancy of less than 10% for any value of PGA. Once the PSDM approach was verified, the authors used the approach to generate fragility curves for all 20 bridge archetypes at each of the three damage limit states. Table 6 features the parameters of the curves relating to the collapse mechanism of spandrel-wall rotation, and Table 7 features the parameters of the curves relating to the relative displacement between the arch crown and the abutment.

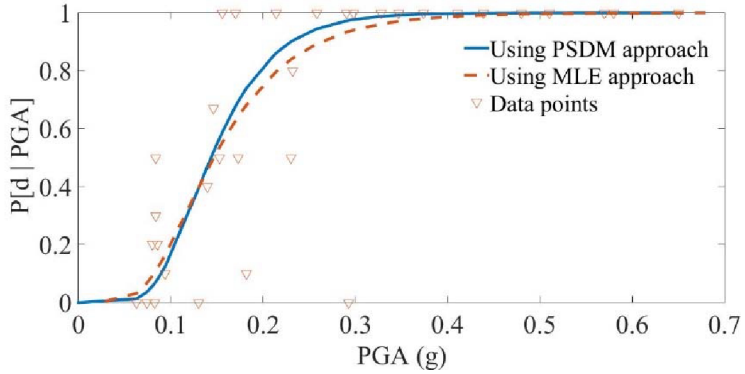

Figure 16 : Comparison of two fragility curves (i.e., PSDM-generated and MLE-generated) for bridge archetype 1 in connection with the collapse mechanism of spandrel-wall rotation.

Table 6: Fragility curve parameters for 20 bridge archetypes at three damage limit states (i.e., slight, moderate, and extensive) corresponding to spandrel-wall rotation

Bridge Archetype	β	Damage Type - Rotation of Spandrel Wall (mm)		
		01 (Slight)	d_2 (Moderate)	0_3 (Extensive)
1	0.14366	0.1436	0.2169	0.3277
2	0.05601	0.0560	0.0999	0.1784
3	0.3674	0.3671	0.6010	0.9832
4	0.1869	0.1869	0.2846	0.4335
5	0.2201	0.2201	0.4092	0.7606
6	0.1379	0.1379	0.2187	0.3468
7	0.0226	0.0226	0.0478	0.1013
8	0.0306	0.0306	0.0572	0.1069
9	0.138	0.1380	0.1892	0.2595
10	0.1189	0.1189	0.2126	0.3801
11	0.1137	0.1137	0.1992	0.3489
12	0.0861	0.0861	0.1352	0.2122
13	0.0155	0.0155	0.0296	0.0567
14	0.1948	0.1948	0.3106	0.4952
15	0.1072	0.1072	0.1744	0.2836
16	0.0116	0.0116	0.0273	0.0645
17	0.1295	0.1295	0.2150	0.3569
18	0.0874	0.0874	0.1461	0.2453
19	0.0685	0.0685	0.2370	0.4481
20	0.2025	0.2025	0.3796	0.7115

Table 7: Fragility curve parameters for 20 bridge archetypes at three damage limit states (i.e., slight, moderate, and extensive) corresponding to relative displacement of arch crown and abutment

Bridge Archetype	β	Damage Type – Relative Displacement Crown vs Abutment		
		0i (Slight)	0_2 (Moderate)	0_3 (Extensive)
1	1.1033	0.4368	0.8613	1.2813
2	0.2717	0.5716	1.1137	1.6452
3	0.4649	0.3245	0.5625	0.9750
4	0.5332	0.5022	0.7926	1.0350
5	0.60038	0.3420	0.5978	0.8287
6	0.7250	0.4002	0.6109	0.7823
7	0.9524	0.3361	0.7356	1.1631
8	0.3884	1.0514	2.6583	4.5735
9	0.6222	0.3802	0.5249	0.6338
10	0.4301	0.4867	0.9559	1.4186

11	0.8473	0.4902	0.7901	1.2734
12	0.9156	0.4811	0.8321	1.4389
13	0.5724	0.2338	0.5207	1.1596
14	0.4091	0.4048	0.5529	0.7551
15	0.7560	0.4596	0.7283	1.1538
16	0.7398	0.6645	1.6247	3.9723
17	0.5497	0.1386	0.2850	0.5859
18	0.2940	0.3927	0.7449	1.4130
19	0.5494	0.6272	1.6043	4.1034
20	0.4664	0.0882	0.1654	0.3101

7. **Seismic Risk Index**

Risk indices were generated for each of the 326 masonry arch bridges by combining the local seismic hazard developed by the USGS (2012) with the corresponding fragility curves for the relevant bridge archetype. Using the location coordinates of the bridges, the PGA values corresponding to each bridge were calculated from the seismic hazard maps shown in Figure 10. Using these values, the probability of damage (i.e., the risk index) for each bridge was obtained from the bridge's representative fragility curves for the two collapse mechanisms. It is important to emphasize that the risk indices developed in this study represented each bridge's probability of failure only when the bridge was subjected to its local seismic hazard.

Damage limit state 1 (i.e., slight) was selected to generate indices as it, among the three damage states, has the maximum probability of occurring. The authors next developed risk maps using ArcGIS 10.3 software. To develop these maps, the collapse mechanism with the higher probability of occurring in damage state 1 was selected. For some bridges, the first collapse mechanism (i.e., relevant displacement of arch crown and abutment) had a higher probability of occurring, but for other bridges, the second collapse mechanism (i.e., spandrel-wall rotation) had a higher probability. Furthermore, the risk index with maximum probability out of two collapse mechanism for damage state 1 is selected to develop risk maps using ArcGIS 10.3 software. Figure 17 illustrates the geographical distribution of risk indices for the probability of failure of the 326 single-span masonry arch bridges for 2% probability of exceedance in the next 50 years. Meanwhile, Figure 18 illustrates the geographical distribution of risk indices for the probability of failure of the same bridges for 10% probability of exceedance in the same time period.

It is important to note that these risk indices do not consider the *consequences* of masonry arch failure. For instance, repair and reconstruction costs and secondary costs caused by disruption in the traffic network are not accounted for in the aforementioned analysis.

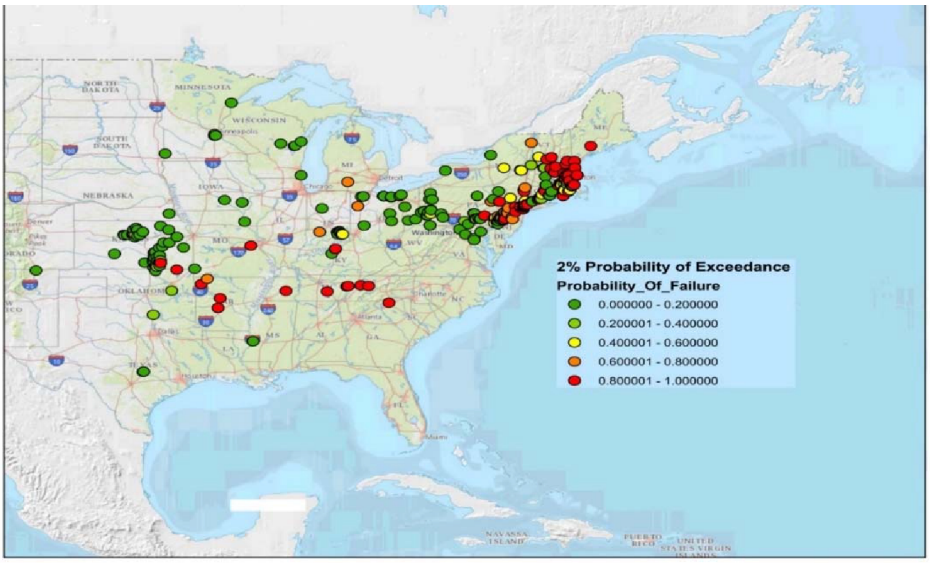

Figure 17 : Geographical distribution of risk indices for 326 single-span masonry arch bridges for damage limit state 1 (i.e., slight) with 2% probability of exceedance in the next 50 years.

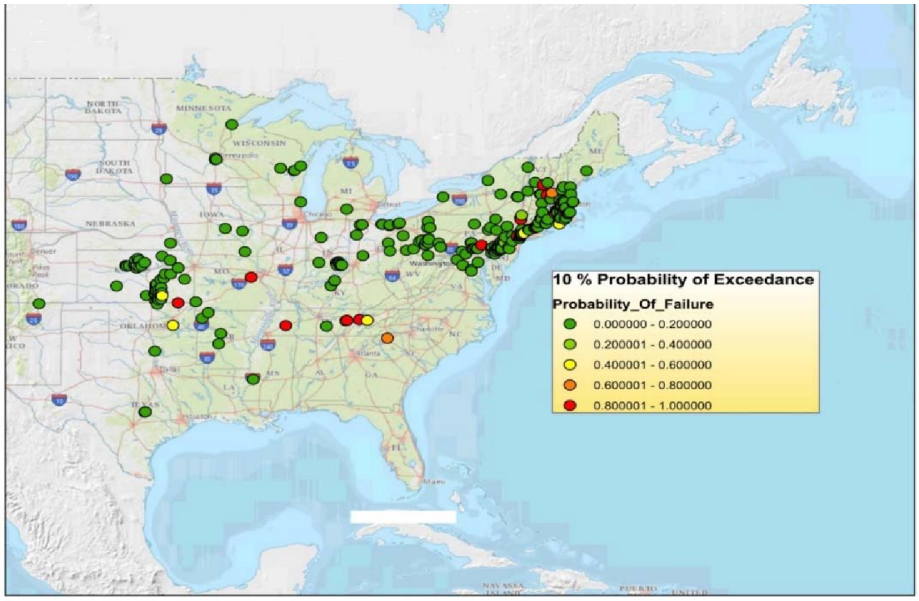

Figure 18 : Geographical distribution of risk indices for 326 single-span masonry arch bridges for damage limit state 1 (i.e., slight) with 10% probability of exceedance in the next 50 years.

The indices generated offer foresight into the seismic risks associated with the 326 bridges. From a preservation perspective, stewards of historic bridges can use these seismic risk indices to develop retrofit strategies that minimize risk of failure and thus reduce financial losses over time. It is estimated that 43.5% of the 326 bridges have a 50% chance of reaching damage limit state 1 (i.e., slight) during a once-in-2475-year earthquake (2% exceedance probability in 50 years).

Meanwhile, 11.7% of the bridges have a 50% chance of reaching damage limit state 1 (i.e., slight) during a once-in-475-year earthquake (10% exceedance probability in 50 years).

8. Conclusion

This study conducted a seismic fragility analysis on a set of representative bridge archetypes to investigate the seismic vulnerability of single-span masonry arch bridges in the U.S. The aim of the study was to encourage risk-aware decisions regarding the bridges' restoration and rehabilitation prior to future seismic activity. The NBI inventory was consulted to gather geometric data for the existing bridges, and 20 representative bridges archetypes were obtained using a *k-means* clustering technique. Non-linear FE models of the archetypes were developed and then used in a Monte-Carlo simulation to obtain fragility curves. The variables of the models were the geometric properties of the bridges. Using synthetic ground motions derived from actual ground motion records for the NMSZ, the authors performed fragility analysis on each of the archetypes in connection with two collapse mechanisms: the relative displacement of the arch crown and the abutment and the rotation of the spandrel wall. By combining the fragility curves for the bridge archetypes and the local seismic hazard for each of the 326 actual bridges, the authors subsequently developed seismic risk indices for each of the actual bridges. The results of this process indicated that spandrel-wall rotation during a seismic event was more likely to result in bridge failure than was the relative displacement of arch crown and abutment.

The major contributions of this study are twofold. First, we productively developed PSDM equations. Second, we created previously nonexistent seismic fragility curves for single-span masonry arch bridges in the central and northeastern regions of the U.S. regions. The results of this study can improve stewardship of masonry arch bridges and can enable a more risk-aware decision process regarding the preservation and rehabilitation of the bridges. Finally, the method used in this study, though focused on single-span masonry arch bridges, can be usefully applied to bridges of other types, provided the geometric properties and local seismic hazards for those bridges are taken into account. For future research, the authors would encourage several areas of study. First, the seismic vulnerability of masonry bridges with two or more spans could be assessed. Second, because no damage limit states exist for masonry arch bridges, as opposed to concrete bridges, future studies could develop quantitative limit states for these bridges as a means of accurately determining fragility functions. Third, future studies could adopt a micro-modeling technique to capture the response of masonry arch bridges to seismic activity. Such a technique could model the mortar joints within a bridge's masonry assembly and could define spring supports using stiffness coefficients at the bottom and two ends of a bridge. Finally, risk indices could be developed that take into account both the cost of bridge replacement or rehabilitation and the overall impact of the failure of masonry arch bridges on the U.S. transportation network.

9. References

1. Aldrich, John. "RA Fisher and the making of maximum likelihood 1912-1922." *Statistical Science* 12, no. 3 (1997): 162-176.
2. ANSYS® Academic Research. Release 15.0. *Help System, Element Reference* ANSYS, Inc
3. Betti, Michele, and Luciano Galano. "Seismic analysis of historic masonry buildings: the vicarious palace in Pescia (Italy)." *Buildings* 2, no. 2 (2012): 63-82.
4. Bhatti, Abdul Qadir. "Seismic vulnerability of historical arch type bridge structures in Italy." PhD diss., Universitat Politècnica de Catalunya. Escola Tècnica Superior d'Enginyers de Camins, Canals i Ports de Barcelona, 2009 (Advanced Masters in Structural Analysis of Monuments and Historical Constructions (SAMHC)), 2009.
5. Bholowalia, Purnima, and Arvind Kumar. "EBK-means: A clustering technique based on elbow method and k-means in WSN." *International Journal of Computer Applications* 105, no. 9 (2014).
6. Bignell, John L., James M. Lafave, Joseph P. Wilkey, and Neil M. Hawkins. "Seismic evaluation of vulnerable highway bridges with wall piers on emergency routes in southern illinois." In *13th world conference on eartquake engineering, Vancouver, BC, Canada*. 2004.
7. Bui, T.T., Limam, A., David, B., Ferrier, E. and Brun, M., 2010, July. Masonry walls submitted to out-of-plane loading: Experimental and numerical study. In *8th International Masonry Conference* (Vol. 2, No. F-243, pp. 1153-1162).
8. Calvi, G. Michele, Rui Pinho, Guido Magenes, Julian J. Bommer, L. Fernando Restrepo-Vélez, and Helen Crowley. "Development of seismic vulnerability assessment methodologies over the past 30 years." *ISET journal of Earthquake Technology* 43, no. 3 (2006): 75-104.
9. CHAJES, MICHAEL. "Load Rating of Arch Bridges." *Final report submitted to Delaware Center for Transportation* (2002).
10. Choi, Eunsoo. "Seismic analysis and retrofit of mid-America bridges." PhD diss., School of Civil and Environmental Engineering, Georgia Institute of Technology, 2002.
11. Citto, C., and D. Woodham. "Evaluation and Rating of Masonry Arch Bridges." In *Structures Congress 2014*, pp. 528-539. 2014.
12. Cornell, C. Allin, Fatemeh Jalayer, Ronald O. Hamburger, and Douglas A. Foutch. "Probabilistic basis for 2000 SAC federal emergency management agency steel moment frame guidelines." *Journal of structural engineering*128, no. 4 (2002): 526-533.
13. da Porto, Francesca, Giovanni Tecchio, Paolo Zampieri, Claudio Modena, and Andrea Prota. "Simplified seismic assessment of railway masonry arch bridges by limit analysis." *Structure and Infrastructure Engineering* 12, no. 5 (2016): 567-591.
14. De Santis, Stefano. "Load-carrying capability and seismic assessment of masonry bridges." PhD diss., Ph. D. Dissertation, 2011.
15. DeJong, Matthew Justin. "Seismic assessment strategies for masonry structures." PhD diss., Massachusetts Institute of Technology, 2009.
16. Ding, Chris, and Xiaofeng He. "K-means clustering via principal component analysis." In *Proceedings of the twenty-first international conference on Machine learning*, p. 29. ACM, 2004.
17. Drucker, Daniel Charles, and William Prager. "Soil mechanics and plastic analysis or limit design." *Quarterly of applied mathematics* 10, no. 2 (1952): 157-165.
18. Fanning, Paul J., and Thomas E. Boothby. "Three-dimensional modelling and full-scale testing of stone arch bridges." *Computers & Structures* 79, no. 29 (2001): 2645-2662.
19. Fanning, Paul J., Thomas E. Boothby, and Benjamin J. Roberts. "Longitudinal and transverse effects in masonry arch assessment." *Construction and Building Materials* 15, no. 1 (2001): 51-60.

20. FHWA “National Bridge Inventory Data” (2012)
21. Field, Edward H. "Probabilistic seismic hazard analysis (PSHA): A primer." *Retrieved May* 17 (2005): 2011.
22. Gan, Guojun, Chaoqun Ma, and Jianhong Wu. *Data clustering: theory, algorithms, and applications*. Society for Industrial and Applied Mathematics, 2007.
23. Gerstle, Walter H., and Joao Elias Abdalla. "Finite element meshing criteria for crack problems." In *Fracture Mechanics: Twenty-First Symposium*. ASTM International, 1990.
24. Ghosh, S. K. "Observations from the Bhuj earthquake of January 26, 2001." *PCI JOURNAL* 46, no. 2 (2001): 34-43.
25. Hwang, Howard, John B. Jernigan, and Yang-Wei Lin. "Evaluation of seismic damage to Memphis bridges and highway systems." *Journal of Bridge Engineering* 5, no. 4 (2000): 322-330.
26. Jain, Anil K. "Data clustering: 50 years beyond K-means." *Pattern recognition letters* 31, no. 8 (2010): 651-666.
27. Jernigan, J. B., and H. Hwang. "Development of bridge fragility curves." In *7th US National Conference on Earthquake Engineering*. 2002.
28. Kanungo, Tapas, David M. Mount, Nathan S. Netanyahu, Christine D. Piatko, Ruth Silverman, and Angela Y. Wu. "An efficient k-means clustering algorithm: Analysis and implementation." *IEEE transactions on pattern analysis and machine intelligence* 24, no. 7 (2002): 881-892.
29. Kappos, Andreas J., Gregory G. Penelis, and Christos G. Drakopoulos. "Evaluation of simplified models for lateral load analysis of unreinforced masonry buildings." *Journal of structural Engineering* 128, no. 7 (2002): 890-897.
30. Kawashima, Kazuhiko, Yoshikazu Takahashi, Hanbin Ge, Zhishen Wu, and Jiandong Zhang. "Reconnaissance report on damage of bridges in 2008 Wenchuan, China, earthquake." *Journal of Earthquake Engineering* 13, no. 7 (2009): 965-996.
31. Kawashima, Kazuhiko, Yoshikazu Takahashi, Hanbin Ge, Zhishen Wu, and Jiandong Zhang. "Reconnaissance report on damage of bridges in 2008 Wenchuan, China, earthquake." *Journal of Earthquake Engineering* 13, no. 7 (2009): 965-996.
32. Kim, Sang-Hoon, and Masanobu Shinozuka. "Development of fragility curves of bridges retrofitted by column jacketing." *Probabilistic Engineering Mechanics* 19, no. 1 (2004): 105-112.
33. King, Stephanie A., Anne S. Kiremidjian, Nesrin Basöz, Kincho Law, Mladen Vucetic, Macan Doroudian, Robert A. Olson, John M. Eidinger, Kenneth A. Goettel, and Gerald Horner. "Methodologies for evaluating the socio-economic consequences of large earthquakes." *Earthquake spectra* 13, no. 4 (1997): 565-584.
34. Kodinariya, Trupti M., and Prashant R. Makwana. "Review on determining number of Cluster in K-Means Clustering." *International Journal* 1, no. 6 (2013): 90-95.
35. Kwasniewski, Slawek, Haakon Hop, Stig Falk-Petersen, and Gunnar Pedersen. "Distribution of Calanus species in Kongsfjorden, a glacial fjord in Svalbard." *Journal of plankton research* 25, no. 1 (2003): 1-20.
36. Lagomarsino, Sergio, and Serena Cattari. "PERPETUATE guidelines for seismic performance-based assessment of cultural heritage masonry structures." *Bulletin of Earthquake Engineering* 13, no. 1 (2015): 13-47.
37. Lallemant, David, Anne Kiremidjian, and Henry Burton. "Statistical procedures for developing earthquake damage fragility curves." *Earthquake Engineering & Structural Dynamics* 44, no. 9 (2015): 1373-1389.
38. Lang, Kerstin. *Seismic vulnerability of existing buildings*. No. 273. vdf Hochschulverlag AG, 2002.
39. Li, Tun, and Sez Atamturktur. "Fidelity and robustness of detailed micromodeling, simplified micromodeling, and macromodeling techniques for a masonry dome." *Journal of Performance of Constructed Facilities* 28, no. 3 (2013): 480-490.

40. Loo, Yew-Chaye, and Yan Yang. "Cracking and failure analysis of masonry arch bridges." *Journal of structural engineering* 117, no. 6 (1991): 1641-1659.
41. Lourenço, Paulo B. "Computations on historic masonry structures." *Progress in Structural Engineering and Materials* 4, no. 3 (2002): 301-319.
42. Mackie, Kevin, and Božidar Stojadinović. "Probabilistic seismic demand model for California highway bridges." *Journal of Bridge Engineering* 6, no. 6 (2001): 468-481.
43. Mander, John B., and Nesrin Basöz. "Seismic fragility curve theory for highway bridges." In *Optimizing post-earthquake lifeline system reliability*, pp. 31-40. ASCE, 1999.
44. Melchers, Robert E. *Structural reliability: analysis and prediction*. Horwood, 1987.
45. Musmar, Mazen A. "Analysis of Shear Wall with Openings Using Solid 65 Element." *Jordan journal of civil engineering* 7, no. 2 (2013): 164-173.
46. Ng, K. H., C. A. Fairfield, and A. Sibbald. "Finite-element analysis of masonry arch bridges." *Proceedings of the Institution of Civil Engineers. Structures and buildings* 134, no. 2 (1999): 119-127.
47. Nielson, Bryant G. "Analytical fragility curves for highway bridges in moderate seismic zones." PhD diss., Georgia Institute of Technology, 2005.
48. Nielson, Bryant, and Reginald DesRoches. "Seismic fragility curves for bridges: A tool for retrofit prioritization." In *Advancing mitigation technologies and disaster response for lifeline systems*, pp. 1060-1070. 2003.
49. Nilsson, Emily Michelle. "Seismic risk assessment of the transportation network of Charleston, SC." PhD diss., Georgia Institute of Technology, 2008.
50. Padgett, Jamie E., and Reginald DesRoches. "Methodology for the development of analytical fragility curves for retrofitted bridges." *Earthquake Engineering & Structural Dynamics* 37, no. 8 (2008): 1157-1174.
51. Padgett, Jamie E., Bryant G. Nielson, and Reginald DesRoches. "Selection of optimal intensity measures in probabilistic seismic demand models of highway bridge portfolios." *Earthquake Engineering & Structural Dynamics* 37, no. 5 (2008): 711-725.
52. Park, Duhee, and Youseef MA Hashash. "Evaluation of seismic site factors in the Mississippi Embayment. II. Probabilistic seismic hazard analysis with nonlinear site effects. " Soil Dynamics and Earthquake Engineering 25, no 2 (2005): 145-156
53. Pelà, Luca, Alessandra Aprile, and Andrea Benedetti. "Comparison of seismic assessment procedures for masonry arch bridges." *Construction and Building Materials* 38 (2013): 381-394.
54. Pellegrino, Carlo, Mariano A. Zanini, Paolo Zampieri, and Claudio Modena. "Contribution of in situ and laboratory investigations for assessing seismic vulnerability of existing bridges." *Structure and Infrastructure Engineering* 11, no. 9 (2015): 1147-1162.
55. Porter, Keith. "Beginner's guide to fragility, vulnerability, and risk." *Encyclopedia of Earthquake Engineering* (2015): 235-260.
56. Ramanathan, Karthik, Reginald DesRoches, and Jamie Padgett. "Analytical fragility curves for multispan continuous steel girder bridges in moderate seismic zones." *Transportation Research Record: Journal of the Transportation Research Board* 2202 (2010): 173-182.
57. Rezaeian, Sanaz, and Armen Der Kiureghian. "Simulation of synthetic ground motions for specified earthquake and site characteristics." *Earthquake Engineering & Structural Dynamics* 39, no. 10 (2010): 1155-1180.
58. Rojahn, Christopher, and Roland L. Sharpe. *Earthquake damage evaluation data for California*. Applied technology council, 1985.
59. Rota, M., Alain Pecker, D. Bolognini, and R. Pinho. "A methodology for seismic vulnerability of masonry arch bridge walls." *Journal of Earthquake Engineering* 9, no. sup2 (2005): 331-353.
60. Rota, M., Alain Pecker, D. Bolognini, and R. Pinho. "A methodology for seismic vulnerability of masonry arch bridge walls." *Journal of Earthquake Engineering* 9, no. sup2 (2005): 331-353.

61. Rota, Maria. "Seismic vulnerability of masonry arch bridge walls." *Yüksek Lisans Tezi, Pavia Universitesi* (2004).
62. Sabatini, P. J., R. C. Bachus, P. W. Mayne, James A. Schneider, and T. E. Zettler. *Geotechnical engineering circular no. 5: evaluation of soil and rock properties*. No. FHWA-IF-02-034. 2002.
63. Sarhosis, Vasilis, Stefano De Santis, and Gianmarco de Felice. "A review of experimental investigations and assessment methods for masonry arch bridges." *Structure and Infrastructure Engineering* 12, no. 11 (2016): 1439-1464.
64. Scheibmeir, Elisabeth. "Nonlinear Seismic Analysis of a Masonry Arch Bridge." *MSc, Universitat Politècnica de Catalunya* (2012).
65. Schwarz, Gideon. "Estimating the dimension of a model." *The annals of statistics* 6, no. 2 (1978): 461-464.
66. Schwer, Leonard E. "Is your mesh refined enough? Estimating discretization error using GCI." *7th LS-DYNA Anwenderforum* 1, no. 1 (2008): 50.
67. Seo, Junwon. "Seismic vulnerability assessment of a family of horizontally curved steel bridges using response surface metamodels." (2009).
68. Sevim, Barış, Alemdar Bayraktar, Ahmet Can Altunişik, Sezer Atamtürktür, and Fatma Birinci. "Assessment of nonlinear seismic performance of a restored historical arch bridge using ambient vibrations." *Nonlinear Dynamics*63, no. 4 (2011): 755-770.
69. Shinozuka, Masanobu, Maria Q. Feng, Jongheon Lee, and Toshihiko Naganuma. "Statistical analysis of fragility curves." *Journal of engineering mechanics* 126, no. 12 (2000): 1224-1231.
70. Shinozuka, Masanobu, Youwei Zhou, Sang-Hoon Kim, Yuko Murachi, Swagata Banerjee, Sunbin Cho, and Howard Chung. "Socio-economic effect of seismic retrofit implemented on bridges in the Los Angeles highway network." *Final Report to the California Department of Transportation* (2005).
71. Taghikhany, T., M. Tehranizadeh, and M. Arabameri. "Vulnerability of Hybrid Masonry Building under Seismic Action." In *The 14th World Conference on Earthquake Engineering. Beijing: Tsinghua University Press*. 2008.
72. Tecchio, G., P. Zampieri, F. da Porto, C. Modena, A. Prota, and G. Manfredi. "Simplified assessment of railway masonry bridges seismic capacity." In *Proceedings of 15th world conference on earthquake engineering (WCEE), September*, pp. 24-28. 2012.
73. Tecchio, Giovanni, Marco Donà, and Francesca da Porto. "Seismic fragility curves of as-built single-span masonry arch bridges." *Bulletin of Earthquake Engineering* 14, no. 11 (2016): 3099-3124.
74. Tsurumaki, Eimitsu. 2016. *Announcing IAC News 50th Issue From 'Information' to 'Intelligence'*. Japan Society of Civil Engineers.
75. USGS (2002), "Earthquake in the heart of homeland" Fact Sheet FS-131-02, U.S. Geological Survey
76. USGS (2017). National Seismic Hazard Maps. Retrieved from https://earthquake.usgs.gov/hazard/hazmaps/
77. Vamvatsikos, Dimitrios, and C. Allin Cornell. "Incremental dynamic analysis." *Earthquake Engineering & Structural Dynamics* 31, no. 3 (2002): 491-514.
78. Vasconcelos, G., and Paulo B. Lourenço. "In-plane experimental behavior of stone masonry walls under cyclic loading." *Journal of structural engineering* 135, no. 10 (2009): 1269-1277.
79. Wang, J., and C. Melbourne. "Finite element analyses of soil-structure interaction in masonry arch bridges." In *Proceedings of the 5th international conference on arch bridges ARCH*, vol. 7, pp. 515-23. 2007.
80. Wang, Junzhe. "Numerical modelling of masonry arch bridges: Investigation of spandrel wall failure." PhD diss., University of Bath, 2014.

81. Wen, Y. K., and B. R. Ellingwood. "The role of fragility assessment in consequence-based engineering." *Earthquake Spectra* 21, no. 3 (2005): 861-877.
82. Wen, Y. K., and Chiun-Lin Wu. "Uniform hazard ground motions for mid-America cities." *Earthquake spectra* 17, no. 2 (2001): 359-384.
83. Whitman, Robert V., Erik H. Vanmarcke, Richard L. de Neufville, J. E. I. Brennan, C. Allin Cornell, and John M. Biggs. "Seismic design decision analysis." *Journal of the Structural Division* 101, no. 5 (1975): 1067-1084.
84. Wu, Lufang. *Serviceability assessments of masonry arch bridges*. Cardiff University (United Kingdom), 2010.
85. Zampieri, P., Tecchio, G., Da Porto, F. and Modena, C., 2015. Limit analysis of transverse seismic capacity of multi-span masonry arch bridges. *Bulletin of Earthquake Engineering*, *13*(5), pp.1557-1579.
86. Zampieri, Paolo, Mariano Angelo Zanini, and Flora Faleschini. "Derivation of analytical seismic fragility functions for common masonry bridge types: methodology and application to real cases." *Engineering Failure Analysis* 68 (2016): 275-291.
87. Zampieri, Paolo. "Semplified seismic Vulnerability Assessment of Masonry Arch Bridges." PhD diss., University of Trento, 2014.
88. Zhang, Yanyang. "Advanced nonlinear analysis of masonry arch bridges." (2015).
89. Luco, Nicolas, and Paolo Bazzurro. "Does amplitude scaling of ground motion records result in biased nonlinear structural drift responses?." *Earthquake Engineering & Structural Dynamics* 36, no. 13 (2007): 1813-1835.
90. Lu, J., Atamturktur, S. and Huang, Y. (2016), "Bi-level resource allocation framework for retrofitting bridges in a transportation network." *Transportation Research Record: Journal of the Transportation Research Board*, Vol. 2550, pp. 31-37.
91. Prabhu, S.* and Atamturktur, S. (2013), "Feature Assimilation for Vibration Based Damage Detection," *Journal of Nondestructive Testing and Evaluation (ASTM)*, Vol. 41, No. 1, pp. 39-49.
92. Ural, Ali, Şeref Oruç, Adem Doğangün, and Ö. İskender Tuluk. "Turkish historical arch bridges and their deteriorations and failures." *Engineering Failure Analysis* 15, no. 1 (2008): 43-53.
93. Atamturktur, S., Hemez, F. and Laman, J. (2012), "Uncertainty Quantification in Model Verification and Validation as Applied to Large Scale Historic Masonry Monuments," *Engineering Structures (Elsevier)*, Vol. 43, pp. 221-234.
94. Fanning, Paul J., Thomas E. Boothby, and Benjamin J. Roberts. "Longitudinal and transverse effects in masonry arch assessment." *Construction and Building Materials* 15, no. 1 (2001): 51-60.
95. Atamturktur, S., Li, T.*, Ramage, M. and Farajpour, I.* (2012), "Load Carrying Capacity Assessment of a Scaled Masonry Dome: Simulations Validated with Non-destructive and Destructive Measurements ," *Construction and Building Materials (Elsevier)*, Vol. 34, pp. 418–429.
96. Li, T.* and Atamturktur, S. (2014), "Fidelity and Robustness of Detailed Micromodeling, Simplified Micromodeling and Macromodeling Techniques for a Masonry Dome," *Journal of Performance of Constructed Facilities (ASCE)*, Vol 28, No. 3, pp. 480-490.
97. Prabhu, S.*, Atamturktur, S., Brosnan, D., Dorrance, R. and Messier, P. (2014), "Foundation Settlement Analysis of Fort Sumter National Monument: Model Development and Predictive Assessment," *Engineering Structures (Elsevier)*, Vol. 65, pp. 1-12
98. Prabhu, S.*, Atamturktur, S. and Cogan, S. (2017), "Model assessment in scientific computing: Considering robustness to uncertainty in input parameters. *Engineering Computations*, Vol. *34*, No. 5, pp. 1700-1723.

99. Prabhu, S.*, Atamturktur, S., Brosnan, D., Dorrance, R. and Messier, P. (2014), "Foundation Settlement Analysis of Fort Sumter National Monument: Model Development and Predictive Assessment," *Engineering Structures (Elsevier)*, Vol. 65, pp. 1-12.
100. Li, T.* and Atamturktur, S. (2014), "Fidelity and Robustness of Detailed Micromodeling, Simplified Micromodeling and Macromodeling Techniques for a Masonry Dome," *Journal of Performance of Constructed Facilities (ASCE)*, Vol 28, No. 3, pp. 480-490.
101. Atamturktur, S., Hemez, F. and Laman, J. (2012), "Uncertainty Quantification in Model Verification and Validation as Applied to Large Scale Historic Masonry Monuments," *Engineering Structures (Elsevier)*, Vol. 43, pp. 221-234.
102. Sabatini, P. J., R. C. Bachus, P. W. Mayne, James A. Schneider, and T. E. Zettler. *Geotechnical engineering circular no. 5: evaluation of soil and rock properties*. No. FHWA-IF-02-034. 2002.
103. Box, George EP. "Non-normality and tests on variances." *Biometrika* 40, no. 3/4 (1953): 318-335.